Available online at www.sciencedirect.com
ScienceDirect
Trans. Nonferrous Met. Soc. China 25(2015) 1248−1253
Transactions of Nonferrous Metals Society of China
www.tnmsc.cn

Selective oxidation of methane to syngas using $Pr_{0.7}Zr_{0.3}O_{2-\delta}$: Stability of oxygen carrier

Yun-peng DU[1,2,3], Xing ZHU[1,2,3], Hua WANG[1,2,3], Yong-gang WEI[1,2,3], Kong-zhai LI[1,2,3]

1. State Key Laboratory of Complex Nonferrous Metal Resources Clean Utilization, Kunming University of Science and Technology, Kunming 650093, China;
2. Faculty of Metallurgy and Energy Engineering, Kunming University of Science and Technology, Kunming 650093, China;
3. Engineering Research Center of Metallurgical Energy Conservation and Emission Reduction, Ministry of Education, Kunming University of Science and Technology, Kunming 650093, China

Received 10 June 2014; accepted 16 November 2014

Abstract: $Pr_{0.7}Zr_{0.3}O_{2-\delta}$ solid solution was prepared by co-precipitation method and used as an oxygen carrier in the selective oxidation of methane to syngas (methane/air redox process). The evolution on the physicochemical properties of $Pr_{0.7}Zr_{0.3}O_{2-\delta}$ during the redox process was studied by means of X-ray diffraction (XRD), H_2 temperature-programmed reduction (H_2-TPR), O_2 temperature-programmed desorption(O_2-TPD), Brunauer-Emmett-Teller (BET) surface area measurement and X-ray photoelectron spectroscopy (XPS) technologies. The results indicated that $Pr_{0.7}Zr_{0.3}O_{2-\delta}$ solid solution showed the high activity for the methane conversion to syngas with a high CO selectivity in the range of 83.5%−88.1%. Though Pr−Zr solid solution possessed high thermal stability, lattice oxygen was obviously reduced for the recycled sample due to decreased surface oxygen which promoted oxygen vacancies. The increased oxygen vacancies seemed to enhance the oxygen transfer ability in the redox process and provided sufficient oxygen for the methane selective oxidation, resulting in a satisfactory activity. The problem of hot pot was avoided by comparing fresh, aged and recycle sample in the reaction.

Key words: methane; selective oxidation; oxygen carrier; Pr−Zr solid solution; syngas; stability

1 Introduction

Methane is an important raw material in the chemical industry, and its conversion to syngas ($CO+H_2$) for further Fischer–Tropsch (F−T) [1,2] or methanol synthesis [3,4] is a major utilization route. Carbon dioxide reforming (CDR), steam methane reforming (SMR) and partial oxidation of methane (POM) [5−7] are the three principal routes for syngas production from methane. Compared with SMR and CDR, POM owns advantages of low capital and operating cost and syngas with a H_2/CO mole ratio of 2.0:1 which is suitable for F−T and methanol synthesis [8]. A novel two-step POM method for selective oxidation of methane to syngas using the lattice oxygen of solid oxides (oxygen carrier) was proposed to avoid explosion risk [9−11]. The most important factor for this method is obtaining oxygen carriers with high activity and stability for the successive redox. As an important oxygen-storage material, praseodymium oxide (Pr_6O_{11}) is reported to own better high-temperature stability than ceria-based oxygen-storage material [12]. The oxygen carriers containing ZrO_2 are sent to the high expectation for its excellent performance at high temperature [13,14]. It is also observed that incorporation of ZrO_2 with Pr_6O_{11} could strongly improve the oxygen mobility due to the formation of Pr_6O_{11}−ZrO_2 solid solution [15]. Therefore, Pr−Zr solid solution is expected to get excellent performance on selective oxidation of methane to syngas process.

In the present work, the stability and durability of $Pr_{0.7}Zr_{0.3}O_{2-\delta}$ as oxygen carrier used in the methane/air redox process were studied for the successive syngas

Foundation item: Projects (51374004, 51174105, 51204083, 51104074, 51306084) supported by the National Natural Science Foundation of China; Projects (2012FD016, 2014HB006) supported by the Applied Basic Research Program of Yunnan Province, China; Project (2010241) supported by the Analysis and Testing Foundation of Kunming University of Science and Technology, China
Corresponding author: Xing ZHU; Tel: +86-871-65153405; E-mail: zhuxing2010@hotmail.com
DOI: 10.1016/S1003-6326(15)63722-0

production. The structural and physicochemical properties of the fresh, recycled and aged $Pr_{0.7}Zr_{0.3}O_{2-\delta}$ were studied by XRD, H_2-TPR, O_2-TPD, BET and XPS technologies for the deep understanding of behavior of Pr−Zr mixed oxide in the selective oxidation of methane for the syngas production.

2 Experimental

2.1 Oxygen carrier preparation

$Pr_{0.7}Zr_{0.3}O_{2-\delta}$ oxygen carrier was prepared by co-precipitation method. The required amounts of $Pr(NO_3)_3{\cdot}6H_2O$ and $Zr(NO_3)_4$ were dissolved in distilled water respectively by magnetic stirring and then mixed with the Pr to Zr molar ratio of 7:3. The surfactant (F127) was added to the solution with mass fraction of 20%. An ammonia solution was gradually added to the mixture with stirring until the pH reached up to 13. The precipitates were washed with distilled water three times after 1 h aging. The result mixtures dried at 110 °C for 24 h and then calcined at 800 °C for 6 h in air.

The aged sample was calcined at 1000 °C for 6 h in air after 800 °C calcination.

2.2 Oxygen carrier characterization

XRD was performed on a Japan Science D/max-R diffractometer using Cu radiation. The X-ray tube was operated at 40 kV and 200 mA. The X-ray diffractogram was recorded at 0.01° interval with a scanning rate of 10 (°)/min for the scanning angle (2θ) from 10° to 90°.

H_2-TPR experiments were performed on a TPR Win v1.50 (produced by Quantachrome Instruments Co.) under a flow of 10% H_2−He mixture (75 cm^3/min) over 100 mg oxygen carrier using a heating rate of 10 °C/min.

O_2-TPD experiments were performed on a TPD Win v1.50 (produced by Quantanchrome Instruments Co.). Under a flow of 10% O_2−N_2 mixture (75 cm^3/min) absorbed at 400 °C for 40 min, 100 mg oxygen carrier was desorbed at a heating rate of 10 °C/min.

The BET surface area was determined by N_2 physisorption using a Quantachrome NOVA 2000e sorption analyzer.

XPS experiments were carried out on a Shimadzu Amicus system equipped with a monochromatic Al K_α X-ray source ($h\nu$=1486.8 eV). Spectra were registered after purging the samples at ambient temperature in vacuum (residual pressure $<10^{-9}$ Pa). An electron flood gun compensated sample charging during the measurement. The electron takeoff angle was 45° with respect to the sample surface. The spectra were referred to the C 1s emission at 284.8 eV.

2.3 Activity test

The selective oxidation of CH_4 was carried out in a continuous flow fixed-bed reactor system under atmospheric pressure. 1.8 g of oxygen carrier was placed in a quartz tube with 15 mm in inside diameter. Prior to catalytic reactions, pure N_2 flowed into the reactor. The oxygen carrier was dried at 300 °C for 2 h under ambient N_2 and then 5% methane flowed into the reactor at 800 °C. The reaction between methane and oxygen carrier was performed at 850 °C. The total gas flow rate of methane was controlled by a mass flow controller at a specific flow rate of 200 cm^3/min. After the isothermal reaction of CH_4 and $Pr_{0.7}Zr_{0.3}O_{2-\delta}$ continued at 850 °C for 60 min, N_2 was introduced into the reactor at a specific flow rate of 50 cm^3/min for 5 min. Then, air was introduced into the reactor to regenerate the reduced oxygen carrier for 30 min. After that, N_2 was imported to purge the reactor for making preparation of next cycle experiment. Reactant and product components were analyzed online by a CO/CO_2 detector (C600, produced by Baoying Technology).

3 Results and discussion

3.1 Cyclic redox performance

In order to study the reaction stability of Pr−Zr oxygen carrier, successive redox process between methane and oxygen carrier was carried out.

Figure 1(a) shows the on-line monitoring information of successive cycles over $Pr_{0.7}Zr_{0.3}O_{2-\delta}$. At the beginning of the reaction for all cycles, a large amount of CO_2 was obtained and then decreased sharply to a really low level in 2 min. The production of CO rose with the decrease of CO_2 evolution, and then kept a stable level for several minutes. This indicated that partial oxidation took place after the exhaustion of surface oxygen for the complete oxidation. After the 10th recycle, CO_2 content was much lower than that of fresh one at the initial stage. Figure 1(b) shows the average contents of CO and CO_2 for successive cycles in 5−20 min. Clearly, CO content did not decrease obviously and the selectivity of CO is 83.5%−88.1% (calculated from the data) after the 10th cycle. Those results revealed that activity of methane selective oxidation was promoted along with the redox process because of modification of physicochemical properties.

3.2 Structure and reducibility evolution

Figure 2 shows the XRD patterns of $Pr_{0.7}Zr_{0.3}O_{2-\delta}$ before and after the 10th recycle. The two patterns represented the typical features of a fluorite-structured Pr_6O_{11} [16]. Compared with the pure Pr_6O_{11}, the diffraction peaks of $Pr_{0.7}Zr_{0.3}O_{2-\delta}$ shifted to higher 2θ positions, while the lattice constant decreases from 0.5453 to 0.5368 nm for the fresh sample. This lattice shrinkage of Pr_6O_{11} should be attributed to the

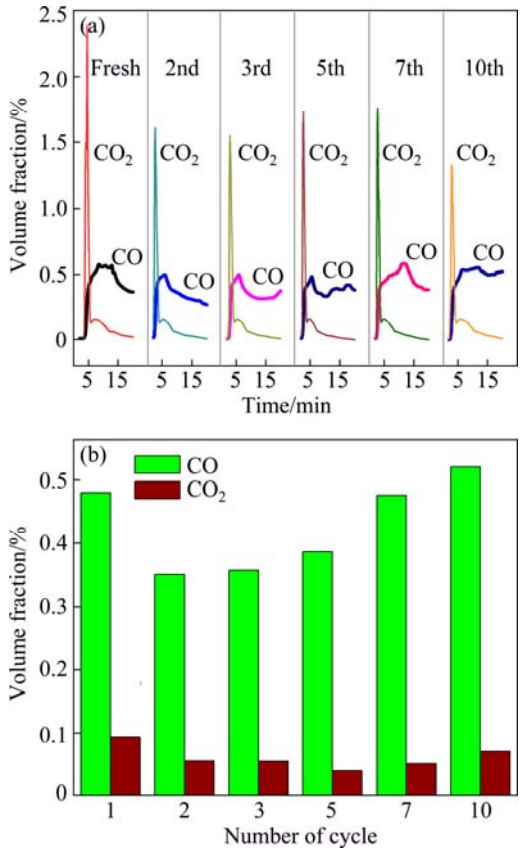

Fig. 1 Effects of successive cycle on catalytic performance of $Pr_{0.7}Zr_{0.3}O_{2-\delta}$: (a) On-line monitoring information; (b) Average data in 5−20 min

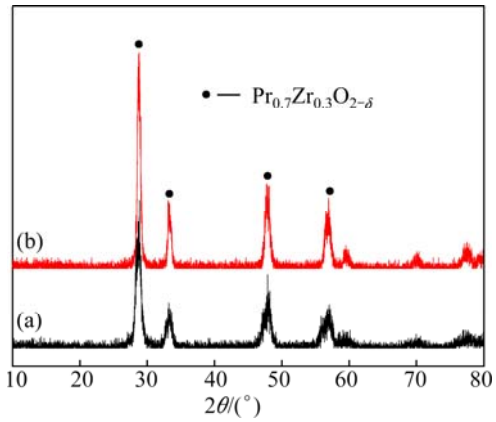

Fig. 2 XRD patterns of fresh sample (a) and 10th recycle sample of $Pr_{0.7}Zr_{0.3}O_{2-\delta}$ (b)

replacement of Pr^{4+} by smaller Zr^{4+} (0.085 vs 0.072 nm for ionic radius) to form Pr_6O_{11}−ZrO_2 solid solution. The effect of successive cycle treatment on the structure of Pr−Zr mixed oxides is not evident from the XRD patterns. After the 10th recycle, no obvious change on the XRD pattern was observed and the crystallite size of Pr_6O_{11} grows a little (10.7 to 11.4 nm from Table 1), indicating high stability of the $Pr_{0.7}Zr_{0.3}O_{2-\delta}$ solid solution.

Table 1 Specific surface area, structural characteristics and H_2-TPR results of tested samples

Sample	Lattice constant of Pr_6O_{11}/nm	Crystallite size of Pr_6O_{11}/nm	BET/ ($m^2 \cdot g^{-1}$)	H_2 consumption/ ($mmol \cdot g^{-1}$)
Fresh	0.5368	10.7	17.4	1.40
10th recycle	0.5385	11.4	9.2	0.69
Aged	0.5350	11.1	12.2	1.32

The reducibility and oxygen distribution of fresh and recycled oxygen carriers were studied by H_2-TPR and O_2-TPD, as shown in Fig. 2. WAN et al [17] reported that the H_2-TPR profile of pure Pr_6O_{11} is characterized by three peaks at 510, 565 and 800 °C, respectively. The high-temperature peak can be attributed to the reduction of bulk lattice, and the low temperature peak and its shoulder are attributed to the two-stage reduction of surface lattice oxygen [18]. Compared with pure Pr_6O_{11}, the reduction peaks of Pr−Zr mixed oxides moved to lower temperatures of 505, 550 and 635 °C (marked as OI, OII and OIII, respectively) after the formation of Pr−Zr solid solution. Since Zr^{4+} is a non-reducible cation [19], the intensity of H_2 consumption is attributed to the reduction from Pr^{4+} to Pr^{3+}. The disappearance of high temperature consumption band should be expected that surface and bulk oxygen was reduced concurrently, because oxygen located within the bulk which may come to the surface when surface oxygen is consumed due to high oxygen mobility [19]. After the 10th recycle, the intensity of OI and OII decreased and OIII disappeared. This may be ascribed to the disappearance of surface oxygen and increased oxygen vacancies after redox treatment.

Figure 3 shows the effects of redox treatment on the oxygen distribution of $Pr_{0.7}Zr_{0.3}O_{2-\delta}$. The two patterns all showed an obvious peak at around 475 °C and two weak peaks at 675 and 865 °C. The low-temperature main peak should be attributed to the desorption of surface oxygen, and the two high-temperature peaks attributed to the two-stage desorption of lattice oxygen [20]. The D1 peak with high intensity indicates that most of the active oxygen in the $Pr_{0.7}Zr0_{.3}O_{2-\delta}$ solid solution could release in inert atmosphere at low temperatures. After redox treatment, the intensity of desorption peak decreased slightly on the O_2-TPD pattern, indicating surface oxygen was consumed during the redox treatment.

The effects of redox treatment on the valency/ oxidation state of elements and surface composition were determined by XPS. The chemical states of Pr and O in the studied samples were identified by fitting the XPS curves (Fig. 4), and the elemental composition and the relative proportion were determined on the basis of the XPS data (Table 2).

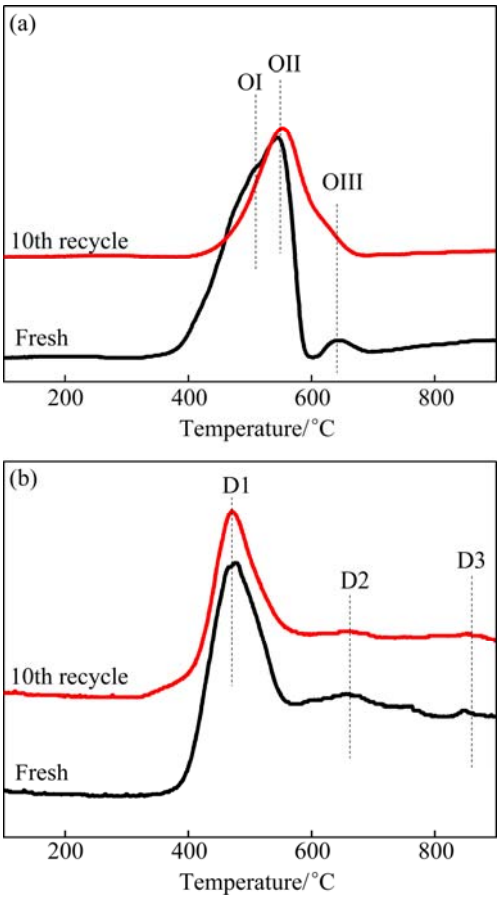

Fig. 3 Effects of redox treatment on H_2-TPR (a) and O_2-TPD (b) patterns of fresh sample and the 10th recycle sample of $Pr_{0.7}Zr0_{.3}O_{2-\delta}$

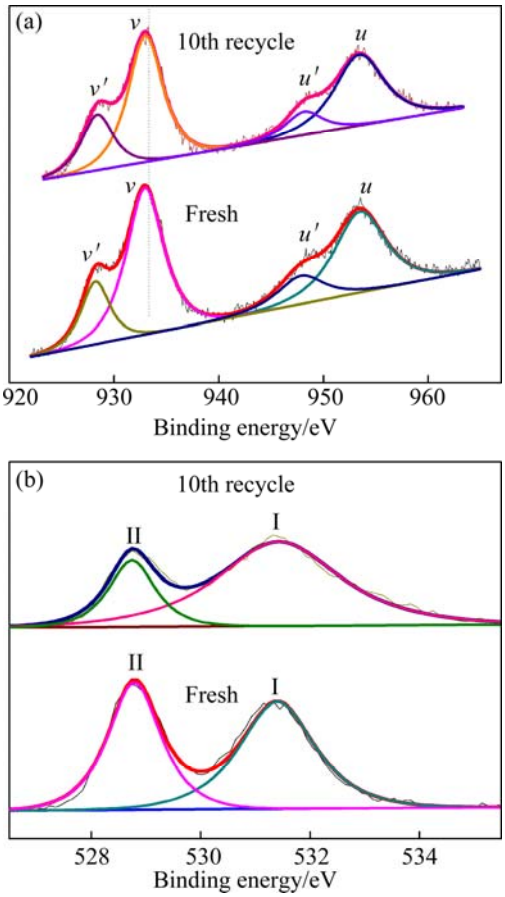

Fig. 4 XPS of Pr 3d (a) and O 1s (b) patterns of fresh sample and 10th recycle sample of $Pr_{0.7}Zr0_{.3}O_{2-\delta}$

Two sets of spin-orbit multiples were observed at the binding energies of about 953.5 and 933.9 eV, which represent the $3d_{3/2}$ and $3d_{5/2}$ electrons of Pr, respectively [21]. According to NARULA et al [22], the signals at about 933.9 eV (v) and 953.5 eV (u) are assigned to Pr^{4+} and the signals at about 929.5 eV (v') and 949.8 eV (u') to Pr^{3+}. As shown in Fig. 4(a), all of the spectra can be fitted with four peaks, indicating the coexistence of Pr^{3+} and Pr^{4+}. The relative proportions of the Pr species were calculated by the area ratio of Pr^{4+} $3d_{5/2}$ (v) to Pr^{3+} $3d_{5/2}$ (v').

The O 1s spectrum of each sample is composed of two over-lapped peaks at about 531.5 and 529.5 eV (denoted as I and II respectively) (Fig. 4(b)). The relative proportions of oxygen species are shown in Table 2. It is reported, that the main bind at about 529.5 eV (II) is the characteristic of the lattice oxygen species and the peak with higher bind energy (I) relates to the defect oxides [23].

From Fig. 4(a) and Table 2, the Pr^{3+} proportion of the 10th recycle sample is higher than that of fresh one, indicating formation of more oxygen vacancies for the recycled sample. In the previous study, we found that

Table 2 Surface elemental composition and relative proportions in samples measured by XPS

Oxygen carrier	Pr species percentage/%		O species percentage/%	
	Pr^{4+}	Pr^{3+}	I	II
Fresh	73.47	26.53	56.3	43.7
10th recycle	71.85	28.15	72.5	27.5

surface lattice oxygen showed high oxidation activity for the total oxidation of methane with products of CO_2 and H_2O, while bulk lattice oxygen preferred to partial oxidation giving products of CO [24]. At the earlier stage of reaction, surface lattice oxygen played a leading role. It oxidized methane not only to CO, but also further to CO_2. After surface lattice oxygen was consumed, CO_2 formation rate was lowered, and CO turned to be the main product. For the fresh sample, the amount of surface lattice oxygen was larger than those of subsequent cycles (Fig. 4(a) and Table 2). Therefore, CO_2 content was much higher than that of other cycles on the first cycle. The increased amount of lattice oxygen in the bulk and enhanced oxygen vacancy on the surface

motivated more CO formation. The decreased H_2 consumption in H_2-TPR should be owing to the consumption of surface oxygen and formation of oxygen vacancies (Fig. 3(a) and Table1).

3.3 Thermal stability

Generally, hot spot is a common problem, which could decrease the reaction activity. In order to study the influence of hot spot during the redox process, the fresh oxygen carrier was aged in atmosphere at 1000 °C for 3 h, and the structure was contrasted with fresh one to confirm whether it is a hot spot or not.

The effects of aging on the XRD patterns of $Pr_{0.7}Zr_{0.3}O_{2-\delta}$ are shown in Fig. 5. Both the fresh and the aged samples show the fluorite-structured diffractogram of Pr_6O_{11}. After aging at 1000 °C, the lattice constant decreased and crystallite size increased slightly, indicating that cation distribution becomes more uniform in the lattice although the grain grows under high temperature calcination.

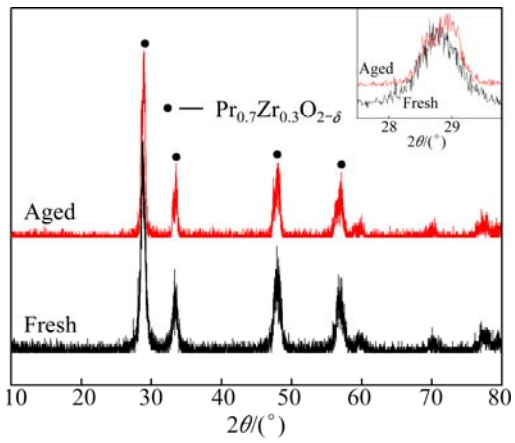

Fig. 5 XRD patterns of fresh and 1000 °C aged $Pr_{0.7}Zr_{0.3}O_{2-\delta}$ samples

Figure 6 shows the H_2-TPR profiles and O_2-TPD results of the fresh and aged $Pr_{0.7}Zr_{0.3}O_{2-\delta}$ samples. Hydrogen reduction peak shifted to high temperatures due to the crystallization of material. No obvious change has been observed for the oxygen distribution in the fresh and recycled samples. In Table 1, it can be found that crystallization degree for recycled sample is slighter than that of the aged one. This result indicated that the problem of hot spot is not obvious and the sintering of martial can be avoided.

4 Conclusions

1) $Pr_{0.7}Zr_{0.3}O_{2-\delta}$ solid solution with co-precipitation method displays favorable activity and stability without hot spot for the selective oxidation of methane to syngas

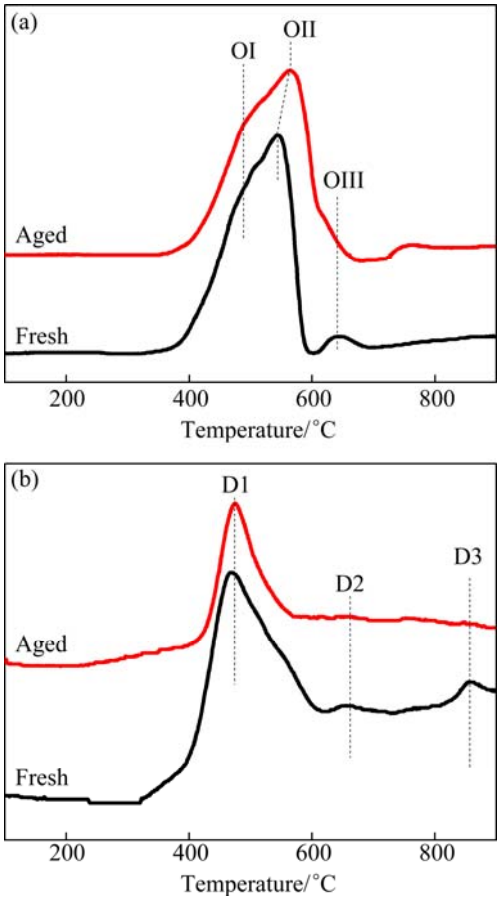

Fig. 6 Effects of aging treatment on H_2-TPR (a) and O_2-TPD (b) patterns of fresh and 1000 °C aged $Pr_{0.7}Zr0_{.3}O_{2-\delta}$ sample

via methane/air redox process. Small variation of surface structure occurs and the whole redox properties are stable in spite of obvious decrease of reducibility of recycled material.

2) Enhanced oxygen vacancies can smoothen the decrease of oxygen capacity of material and provide a constant activity during the syngas production process.

3) Negligible sintering proves that no hot spot occurs during redox process of reduction by methane and oxidation with air.

References

[1] VANDER L G, BEENACKERS A. Kinetics and selectivity of the Fischer−Tropsch synthesis: A literature review [J]. Catalysis Reviews—Science and Engineering, 1999, 41(3−4): 255−318.

[2] HE Fang, WANG Hua, DAI Yong-nian. Preparation and characterization of $La_{0.8}Cu_{0.2}MnO_{(3\pm\delta)}$ perovskite-type catalyst for methane combustion [J]. Transactions of Nonferrous Metals Society of China, 2005, 15(3): 691−696.

[3] TIJM P J A, WALLER F J, BROWN D M. Methanol technology developments for the new millennium [J]. Applied Catalysis A: General, 2001, 221(1−2): 275−282.

[4] CHEN L, ZHANG X W, HUANG L, LEI L C. Partial oxidation of methane with air for methanol production in a post-plasma catalytic system [J]. Chemical Engineering and Processing, 2009, 48(8): 1333−1340.

[5] VAN L F, VANGIEZEN J C, STOBBE E R, GEUS J W. Mechanism of the partial oxidation of methane to synthesis gas on a silica-supported nickel catalyst [J]. Catalysis Today, 1994, 21(2−3): 495−503.

[6] VASANT R C, KARTICK C M. CO_2 reforming of methane combined with steam reforming or partial oxidation of methane to syngas over $NdCoO_3$ perovskite-type mixed metal-oxide catalyst [J]. Applied Energy, 2006, 83(9): 1024−1032.

[7] SALHI N, BOULAHOUACHE A, PETIT C, KIENNEMANN A, RABIA C. Steam reforming of methane to syngas over $NiAl_2O_4$ spinel catalysts [J]. International Journal of Hydrogen Energy, 2011, 36(17): 11433−11439.

[8] LI K Z, WANG H, WEI Y G, YAN D X. Syngas production from methane and air via a redox process using Ce–Fe mixed oxides as oxygen carriers [J]. Applied Catalysis B: Environmental, 2010, 97(3−4): 361−372.

[9] STOBBE E R, BOE B A, GEUS J W. The reduction and oxidation behaviour of manganese oxides [J]. Catalysis Today, 1999, 47(1−4): 161−167.

[10] OTSUKA K, USHIYAMA T, YAMANAKA I. Partial oxidation of methane using the redox of cerium oxide [J]. Chemistry Letters, 1993, 22(9): 1517−1520.

[11] LI K Z, WANG H, WEI Y G, YAN D X. Transformation of methane into synthesis gas using the redox property of Ce−Fe mixed oxides: Effect of calcination temperature [J]. International Journal of Hydrogen Energy, 2011, 36(5): 3471−3482.

[12] LUO M F, YAN Z L, JIN L Y. Structure and redox properties of $Ce_xPr_{1-x}O_{2-\delta}$ mixed oxides and their catalytic activities for CO, CH_3OH and CH_4 combustion [J]. Journal of Molecular Catalysis A: Chemical, 2006, 260(1−2): 157−62.

[13] LUO Qing, CAI Qi-zhou, LI Xin-wei, PAN Zhen-hua, LI Yu-jie, CHEN Xi-di, YAN Qing-song. Preparation and characterization of ZrO_2/TiO_2 composite photocatalytic film by micro-arc oxidation [J]. Transactions of Nonferrous Metals Society of China, 2013, 23(10): 2945−2950.

[14] ZUO Ke, WANG Xin, LIU Wei, ZHAO Yue. Preparation and characterization of Ce−silane−ZrO_2 composite coatings on 1060 aluminum [J]. Transactions of Nonferrous Metals Society of China, 2014, 24(5): 1474−1480.

[15] HE H, DAI H X, WONG K W, AU C T. $RE_{0.6}Zr_{0.4-x}Y_xO_2$ (RE=Ce, Pr; x=0, 0.05) solid solutions: An investigation on defective structure, oxygen mobility, oxygen storage capacity, and redox properties [J]. Applied Catalysis A: General, 2003, 251(1): 61−74.

[16] BELLAKKI M B, SHIVAKUMARA C, BAIDYA T. Synthesis, structure and oxygen-storage capacity of $Pr_{1-x}Zr_xO_{2-\delta}$ and $Pr_{1-x-y}Pd_yZr_xO_{2-\delta}$ [J]. Materials Research Bulletin, 2008, 43(10): 2658−2667.

[17] WAN Y, MA J X, FANG M, LIU Y T. Oxygen storage opacity and adsorptive property of praseodymium oxides [J]. Journal of Rare Earths, 2003, 21(6): 609−612.

[18] LUO M F, YAN Z L, JIN L Y. Structure and redox properties of $Ce_xPr_{1-x}O_{2-\delta}$ mixed oxides and their catalytic activities for CO, CH_3OH and CH_4 combustion [J]. Journal of Molecular Catalysis A: Chemical, 2006, 260(1−2): 157−162.

[19] ATRIBAK I, BUENOLOPEZ A, GARCIAGARCIA A. Combined removal of diesel soot particulates and NO_x over CeO_2−ZrO_2 mixed oxides [J]. Journal of Catalysis, 2008, 259(1): 123−132.

[20] TAKASU Y, MATSUI M, TAMURA H, KAWAMURA S, MATSUDA Y, TOYOSHIMA I. Temperature-programmed desorption on the unstable lattice oxygen of praseodymium oxide [J]. Journal of Catalysis, 1981, 69(1): 51−57.

[21] HE H, DAI H X, WONG K W, AU C T. $RE_{0.6}Zr_{0.4-x}Y_xO_2$ (RE=Ce, Pr; x=0, 0.05) solid solutions: An investigation on defective structure, oxygen mobility, oxygen storage capacity, and redox properties [J]. Applied Catalysis A, 2003, 251(1): 61−74.

[22] NARULA C K, HAACK L P, CHUN W, JEN H W, GRAHAM G W. Single-phase PrO_y−ZrO_2 materials and their oxygen storage capacity: A comparison with single-phase CeO_2−ZrO_2, PrO_y−CeO_2, and PrO_y−CeO_2−ZrO_2 [J]. Materials. Journal of Physical Chemistry B, 1999, 103(18): 3634−3639.

[23] LI K Z, WANG H, WEI Y G, YAN D X. Partial oxidation of methane to syngas with air by lattice oxygen transfer over ZrO_2-modified Ce–Fe mixed oxides [J]. Chemical Engineering Journal, 2011, 173(2): 574−528.

[24] ZHU X, WANG H, WEI Y G, LI K Z, CHENG X M. Hydrogen and syngas production from two-step steam reforming of methane over CeO_2−Fe_2O_3 oxygen carrier [J]. Journal of Rare Earths, 2010, 28(6): 907−913.

$Pr_{0.7}Zr_{0.3}O_{2-\delta}$选择性氧化甲烷制取合成气：氧载体稳定性

杜云鹏[1,2,3]，祝 星[1,2,3]，王 华[1,2,3]，魏永刚[1,2,3]，李孔斋[1,2,3]

1. 昆明理工大学 省部共建复杂有色金属资源清洁利用国家重点实验室，昆明 650093；

2. 昆明理工大学 冶金与能源工程学院，昆明 650093；

3. 昆明理工大学 冶金节能减排教育部工程研究中心，昆明 650093

摘 要：以共沉淀法制备的$Pr_{0.7}Zr_{0.3}O_{2-\delta}$固溶体作为氧载体，研究其在选择性氧化甲烷制取合成气工艺(CH_4/空气氧化还原循环)中的服役性能。结合 X 射线衍射(XRD)、H_2-程序升温还原(H_2-TPR)、O_2-程序升温脱附(O_2-TPD)、比表面测试(BET)、X 射线光电子能谱(XPS)表征手段描述氧载体在氧化还原循环反应过程中物化特性演变。结果表明， $Pr_{0.7}Zr_{0.3}O_{2-\delta}$固溶体在氧化还原反应中保持较高的甲烷反应活性与 CO 选择性，且能够保持反应性能稳定(CO 选择性为 83.5%~83.1%)。随着循环反应的进行，Pr−Zr 固溶体保持了较高的热稳定性，但是表面氧的消失导致其还原性能下降。然而，表面氧的消失促进了氧空位的增加从而在一定程度上增强了氧移动能力，使足够的晶格氧参与到甲烷选择性氧化反应中，保证了较高的反应活性。通过比较新鲜、循环与老化后材料结构与还原性能，认为甲烷选择性氧化制取合成气工艺中的热点问题可以避免。

关键词：甲烷；选择性氧化；氧载体；Pr−Zr 固溶体；合成气；稳定性

(Edited by Xiang-qun LI)